Influence of Reagent Rotation on (H^-, D_2) and (D^-, H_2) Collisions: A Quantum Mechanical Study

Kousik Giri and N. Sathyamurthy*

Department of Chemistry, Indian Institute of Technology Kanpur, Kanpur 208 016, India

Received: May 2, 2006; In Final Form: October 24, 2006

Time-independent quantum mechanical (TIQM) approach (helicity basis truncated at $k = 2$) has been used for computing differential and integral cross sections for the exchange reaction $H^- + D_2$ ($v = 0$, $j = 0-4$) → $HD + D^-$ and $D^- + H_2$ ($v = 0$, $j = 0-3$) → $HD + H^-$ in three dimensions on an accurate ab initio potential energy surface. It is shown that the *j*-weighted differential reaction cross section values are in good agreement with the experimental results reported by Zimmer and Linder at four different relative translational energies ($E_{trans} = 0.55$, 0.93, 1.16 and 1.48 eV) for (H^-, D_2) and at one relative translational energy ($E_{trans} = 0.6$ eV) by Haufler et al. for both (H^-, D_2) and (D^-, H_2) collisions. The *j*-weighted integral reaction cross section values are in good agreement with the crossed beam measurements by Zimmer and Linder in the E_{trans} range 0.5−1.5 eV and close to the guided ion beam results by Haufler et al. for (H^-, D_2) in the range 0.8−1.2 eV. Time-dependent quantum mechanical (TDQM) results obtained using centrifugal sudden approximation are reported in the form of integral reaction cross section values as a function of E_{trans} in the range 0.3−3.0 eV for both reactions in three dimensions on the same potential energy surface. The TDQM reaction cross section values decline more sharply than the TIQM results with increase in the initial rotational quantum number (j) for the D_2 molecules in their ground vibrational state ($v = 0$) for (H^-, D_2) collisions. The computed *j*-weighted reaction cross section values are in good agreement with the experimental results reported by Zimmer and Linder for (H^-, D_2) collisions and guided ion beam results by Haufler et al. for both (H^-, D_2) and (D^-, H_2) collisions for energies below the threshold for electron detachment channel.

I. Introduction

The dynamics of (H^-, H_2) and its isotopic variants has received considerable attention over the years, both experimentally[1−7] and theoretically.[8−20] Although a diatomics-in-molecules (DIM)[8] potential energy surface (PES) and a multireference-configuration-interaction[9] (MRCI) PES were published earlier, Panda and Sathyamurthy[18] have computed recently an ab initio PES using coupled cluster singles and doubles with nonperturbative triples (CCSD(T)) method for a wide range of geometries. An analytic function was fitted to the ab initio points following the strategy proposed by Aguado et al.[21]

Jaquet and Heinen[16] had shown using time-dependent quantum mechanical (TDQM) calculations on DIM and MRCI surfaces that the resonances observed for zero total angular momentum ($J = 0$) got smeared, when averaged over *J*. Morari and Jaquet[17] computed the excitation function for the exchange reaction $H^- + D_2$ ($v = 0$, $j = 0$) → $HD + D^-$ by including Coriolis coupling and found the results to be in agreement with the experimental results of Zimmer and Linder[5] for a range of energies and not with those of Haufler et al. [7] over the same energy range. Panda et al.[19] used the TDQM method with the centrifugal sudden approximation for computing the integral reaction cross section values for (H^-, H_2 ($v = 0$, $j = 0$)), and its isotopic variants. Their results were also found to be in good agreement with the experimental results of Zimmer and Linder[5] but larger than that of Haufler[7] et al. A careful examination of the experimental conditions revealed that Zimmer and Linder had used D_2 that had a rotational temperature of 180 K, and Haufler et al. used D_2 (H_2) with a rotational temperature of 300 K. The theoretical calculations (ours as well as that of Morari and Jaquet) had used $j = 0$ for D_2 (H_2). Therefore, it is possible that some of the discrepancies between theory and experiment arose from the neglect of the effect of the initial rotational state of D_2 (H_2) on the dynamics. Hence, it was decided to investigate the (H^-, D_2) and (D^-, H_2) dynamics by explicitly taking into account the initial rotational state distribution for D_2 (H_2). Recently, the TIQM investigation of the integral and differential cross section of rotational excitation in (H^-, H_2 ($v = 0$, $j = 0$, 1)) collisions have been carried out by Giri and Sathyamurthy.[20] The computed results are in reasonable agreement with the experimental results of Müller et al.[6]

Linder and co-workers[5,6] had published differential reaction cross section results for (H^-, H_2) and (H^-, D_2) collisions. Similarly, Haufler et al. [7] had published differential and integral reaction cross section for (H^-, D_2) and (D^-, H_2) collisions. Therefore, computing the differential reaction cross section values and comparing with the experimental results would test the accuracy of the ab initio PES. Unfortunately, the TDQM method used does not yield information on the product angular distribution. Hence, time-independent quantum mechanical (TIQM) calculations were carried out for computing integral and differential cross sections at $E_{trans} = 0.55$, 0.6, 0.93, 1.16 and 1.48 eV for (H^-, D_2) and at $E_{trans} = 0.6$ eV for (D^-, H_2) collisions, for which the experimental results were available. Three-dimensional TDQM investigations were carried out for integral reaction cross sections in the 0.3−3.0 eV collision energy range for (H^-, D_2 ($v = 0$, $j = 0-4$)) and (D^-, H_2 ($v = 0$, $j = 0-3$)) collisions and these results were also compared

* To whom correspondence should be addressed. E-mail: nsath@iitk.ac.in.

10.1021/jp062675f CCC: $33.50
Published on Web 12/08/2006

with experiment. The theoretical methodology is outlined in section II and the results obtained are presented and discussed in section III. A summary of our findings and the conclusions follow in section IV.

II. Methodology

Time-independent quantum mechanical calculations have been carried out using the ABC program developed by Skouteris et al.[22] in hyperspherical coordinates and the potential energy surface reported by Panda and Sathyamurthy[18] was used. The parity-adapted **S**-matrix elements, $S^{J,P}_{\alpha' v' j' K',\alpha v j k}$, obtained from the TIQM calculations were used to calculate the state-resolved differential cross section values after transformation into their standard helicity representation, $S^{J}_{\alpha' v' j' K',\alpha v j k}$, as

$$\frac{d\sigma_{\alpha' v' j' k' \leftarrow a v j k}}{d\Omega}(\theta) = \left|\frac{1}{2ik_{a v j k}} \sum_J (2J+1) d^J_{k',k}(\theta) S^J_{\alpha' v' j' K',\alpha v j k}\right|^2 \quad (1)$$

and the integral reaction cross section as

$$\sigma_{\alpha' v' j' K' \leftarrow a v j k} = \frac{\pi}{k_{a v j k}{}^2} \sum_J (2J+1) |S^J_{\alpha' v' j' K',\alpha v j k}|^2 \quad (2)$$

where Ω and θ are solid and scattering angles, respectively. α, α', v, v', j, j', k and k' are arrangement labels, diatomic vibrational quantum numbers, diatomic rotational quantum numbers and helicity quantum numbers, respectively. The primed quantities refer to the products of the reaction and unprimed to the reactants.

After extensive convergence tests, a cutoff energy of $E_{max} = 3.5$ eV was used. The maximum rotational level (j_{max}) was taken to be 22, and the maximum value of the hyperradius (ρ_{max}) was set at 20 a_0. The number of log derivative propagation sectors (mtr) = 400. Helicity truncation parameter (k_{max}) was taken up to 2.

Different aspects of the TDQM wave packet (WP) methodology are well documented in the literature.[23,24] Therefore, we present only the salient features of our calculation here. We have used a rectangular grid in Jacobi coordinates (R, r, γ), where R is the center-of-mass separation between H^- (D^-) and D_2 (H_2), r is the bond distance in D_2 (H_2), and γ is the angle between R and r. The Hamiltonian in (R, r, γ) for a given orbital angular momentum operator **l** and rotational angular momentum operator **j** in the body-fixed frame is given by

$$\hat{H} = -\frac{\hbar^2}{2\mu_R}\frac{\partial^2}{\partial R^2} - \frac{\hbar^2}{2\mu_r}\frac{\partial^2}{\partial r^2} + \frac{(\mathbf{J}-\mathbf{j})^2}{2\mu_R R^2} + \frac{\mathbf{j}^2}{2\mu_r r^2} + V(R, r, \gamma) \quad (3)$$

Here μ_R is the reduced mass of H^- (D^-) with respect to D_2 (H_2) and μ_r the reduced mass of D_2 (H_2). Total angular momentum operator $\mathbf{J} = \mathbf{l} + \mathbf{j}$ and V(R, r, γ) is the same interaction potential as mentioned above.[18]

The dynamics of (H^- (D^-)) and (D_2 (H_2)) collisions were followed by solving the time-dependent Schrödinger equation numerically. The initial WP at time $t = 0$, $\Psi(R, r, \gamma, t = 0)$ is chosen as follows:

$$\Psi(R, r, \gamma, t = 0) = G_{k_0}(R)\, \phi_{vj}(r)\, \tilde{P}_{jK}(\cos\gamma) \quad (4)$$

where

$$G_{k_0}(R) = \left(\frac{1}{\pi\delta^2}\right)^{1/4} \exp(-(R-R_0)^2/2\delta^2) \exp(-i_{k_0} R) \quad (5)$$

represents the translational part, with R_0 and δ referring to the location of the center of the WP and the width parameter, respectively. The momentum wave vector k_0 is related to the initial translational energy through the relation[25]

$$k_0 = \sqrt{\frac{2\mu_R E_{trans}}{\hbar^2} - \frac{1}{2\delta^2}} \quad (6)$$

The radial part of the diatomic ro-vibrational eigenfunction $\phi_{vj}(r)$ is computed by the Fourier grid Hamiltonian approach proposed by Marston and Balint-Kurti.[26] The angular part is given by the normalized associated Legendre polynomials

$$\tilde{P}_{jK}(\cos\gamma) = \sqrt{\frac{(2j+1)}{2}\frac{(j-K)!}{(j+K)!}} P_{jK}(\cos\gamma) \quad (7)$$

Here K is the projection of J on the body-fixed z-axis chosen along R and for a given J and j, K varies in the range $0 \le K \le \min(J,j)$. It is worth pointing out here that the projection of j on the body-fixed z-axis is equal to K, as l_z, the projection of l on the body-fixed z-axis is zero, in the chosen body-fixed axis.

The fast Fourier transform algorithm[27] is used to evaluate the effect of the radial part of the kinetic energy operator on the wave function and the discrete variable representation [DVR][28] is used for the angular part. The action of the angular momentum operators (nondiagonal in the radial grid representation) on the WP is carried out in the associated Legendre polynomial basis set $\tilde{P}_{jK}$. First, the WP is transformed to the angular momentum space (finite basis representation (FBR)) by using DVR−FBR transformation matrix, $T^K_{nj} = \sqrt{w_n}\tilde{P}_{jK}(\cos\gamma)$. Then the matrix elements are evaluated as

$$\langle \tilde{P}_{jK}|\mathbf{j}^2|\tilde{P}_{j'K'}\rangle = \delta_{jj'}\delta_{K,K'}\hbar^2 j(j+1) \quad (8)$$

$$\langle \tilde{P}_{jK}|(\mathbf{J}-\mathbf{j})^2|\tilde{P}_{j'K'}\rangle = \hbar^2\delta_{jj'}\{[J(J+1)+j(j+1)-2K^2]\delta_{K,K'} - \lambda^+_{JK}\lambda^+_{jK}\sqrt{1+\delta K_0}\delta_{K+1,K'} - \lambda^-_{JK}\lambda^-_{jK}\sqrt{1+\delta K_1}\,\delta_{K-1,K'}\} \quad (9)$$

where the quantity λ is defined as

$$\lambda^{\pm}_{AB} = \sqrt{A(A+1) - B(B\pm 1)} \quad (10)$$

Within the centrifugal sudden approximation,[29] the off-diagonal terms in K are neglected. The angular kinetic energy operator then reads as

$$\hat{T}(\gamma) = \frac{\hbar^2}{2\mu_R R^2}[J(J+1)+j(j+1)-2K^2] + \frac{\hbar^2}{2\mu_r r^2} j(j+1) \quad (11)$$

The time evolution of the wave function is followed using the split-operator method.[30] The energy resolved reaction probability for a particular choice of v, j, J and K ($P^{JK}_{vj}(E)$) is calculated from the total flux through a surface located in the product channel at $r = r_s$ as follows:[31]

$$P^{JK}_{vj}(E) = \frac{\hbar}{\mu_r}\,\mathrm{Im}\Big[\int_0^\infty dR \int_0^\pi d\theta \sin\theta \Psi^*(R, r, \theta, E)\frac{d}{dr}\Psi(R, r, \theta, E)\Big]_{r=r_s} \quad (12)$$

TABLE 1: Parameters Used for the Rectangular Grid and Initial Conditions

parameters	values	remarks
N_R	150	no. of grid points along R
$(R_{min}, R_{max})/a_0$	(0.05, 17.93)	range of the grid along R
$\Delta R/a_0$	0.12	grid spacing along R
N_r	80	no. of grid points along r
$(r_{min}, r_{max})/a_0$	(0.05, 11.11)	range of the grid along r
$\Delta r/a_0$	0.14	grid spacing along r
N_g	54	no. of grid points in γ
$(R_{mask}, r_{mask})/a_0$	(13.37, 6.91)	starting point of the masking function along (R, r)
R_0/a_0	(12.0)	center of the initial WP
E_{trans}/eV	1.00	initial translational energy
d/a_0	0.25	Gaussian width parameter
r_s/a_0	6.0	position of the flux analysis surface
Δt/fs	0.2419	time-step used in the propagation
T/ps	0.73	total propagation time

The energy dependence of the wave function in eq 12 is obtained by Fourier transforming the time-dependent wave packet as

$$\Psi(R, r, \theta, E) = \frac{1}{a_E}\int_{-\infty}^{\infty} \exp(iEt/\hbar)\, \Psi(R, r, \theta, t)\, dt \qquad (13)$$

with a_E as the normalization factor. The latter corresponds to the weight of the energy component contained in the initial translational WP and is defined by

$$a_E = \left(\frac{\mu_R}{\hbar k}\right)^{1/2} \int_{-\infty}^{\infty} G_{k_0}(R) \exp(ikR)\, dR$$
$$= \left(\frac{\mu_R}{\hbar k}\right)^{1/2} G_{k_0}(k) \qquad (14)$$

Here

$$G_{k_0}(k) = (4\pi\delta^2)^{1/4} \exp[-\delta^2(k - k_0)^2/2 + i(k - k_0)R_0] \qquad (15)$$

with $k = \sqrt{2\mu_R(E-\epsilon_{v,j})}/\hbar$, $\epsilon_{v,j}$ is the ro-vibrational energy of H_2 (D_2).

The J-dependent reaction probability (P^J_{vj}) is computed from the initial (J, K) selected probability (P^{JK}_{vj}) as

$$P^J_{vj}(E) = \frac{1}{2j+1}[P^{JK=0}_{vj}(E) + 2\sum_{K=1}^{j} P^{JK}_{vj}(E)] \qquad (16)$$

The initial-state-selected total reaction cross section values are then obtained by summing over the partial reaction cross section values for the different partial waves:

$$\sigma_{vj}(E) = \frac{\pi}{k^2}\sum_{J=0}^{\infty}(2J+1)P^J_{vj}(E) \qquad (17)$$

A damping function[32] was used near the edges in (R, r) space to avoid numerical errors arising from reflection or wrapping around of time-evolved wave packet at the grid edges. It is given by

$$f(X_i) = \sin\left[\frac{\pi}{2}\frac{(X_{mask} + \Delta X_{mask} - X_i)}{\Delta X_{mask}}\right] \qquad X_i \geq X_{mask} \qquad (18)$$

activated in the asymptotic R and r channels. X_{mask} ($X = R$, r) is the point at which the damping function is initiated and $X_{mask}(=X_{max} - X_{mask})$ is the width of X over which the function decays from 1 to 0, with X_{max} being the maximum value of X in that direction, in a particular channel. The grid parameters used in the present calculation are listed in Table 1 along with the initial conditions, for $J \leq 8$.

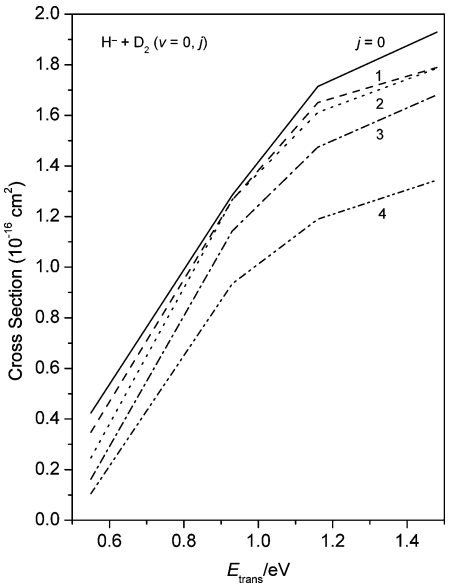

Figure 1. TIQM computed reaction cross section values plotted as a function of E_{trans}/eV for different initial j values for H^-, D_2 ($v = 0$, j) collisions.

Increase in J adds a substantial centrifugal barrier to the interaction potential resulting in an effective potential that falls off slowly and is no longer negligible at distances considered in Table 1. Therefore, the initial WP was located farther out in the reactant channel for higher J values. For $J > 8$, R_0 had to be increased by 1.0 a_0 on an average for each higher J, keeping in mind a cutoff of 0.005 eV for the lowest V_{eff} ($= V(R, r, \gamma) + J(J+1)\hbar^2/2\mu_R R^2$). Consequently, the position of the damping function in the reactant channel also had to be shifted accordingly for each calculation and a longer time evolution of the initial WP was needed to achieve convergence. Converged results were obtained after a total propagation time of 2000−3000 time steps, i.e., 0.48−0.73 ps.

III. Results and Discussion

A. TIQM Results. *A.1. Integral Reaction Cross Sections.* The initial-state-selected reaction cross section values computed using eq 2 are plotted as a function of E_{trans} in the range 0.5−1.5 eV for H^-, D_2 collisions, for different j states of D_2 in Figure 1. It is clear that they rise from the threshold and increase with increase in E_{trans} before showing signs of leveling off. It is also clear from the figure that the cross section values decline with an increase in j from 0 through 3 and 4 over the entire energy range investigated.

This is expected of a reactive collision dominated by collinear configuration.[33] But the differences between the reaction cross section values for $j = 0$, 1 and 2 is marginal. Because the experimental results were obtained for a distribution of j states, the j-weighted integral reaction cross section ($\langle\sigma\rangle$) values were computed as follows:

$$\langle\sigma\rangle = \sum_j w_j(T_{rot.})\sigma_{0j} \qquad (19)$$

where $w_j(T_{rot.})$ is the population of different rotational levels at the rotational temperature $T_{rot.}$. For D_2, the values are 0.299, 0.275, 0.347, 0.057 and 0.021 for $j = 0$−4 corresponding to

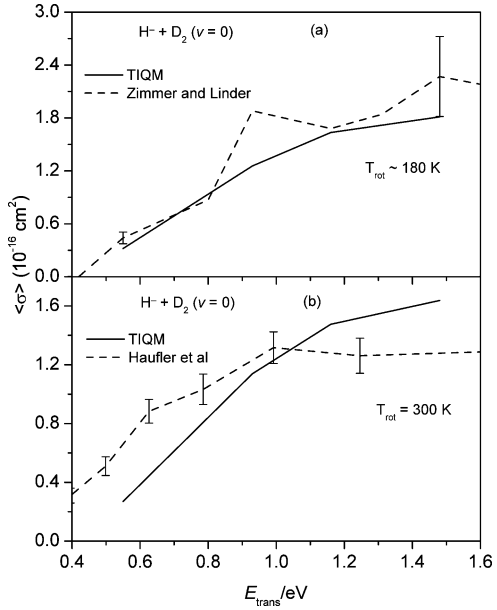

Figure 2. Comparison of the TIQM computed *j*-weighted integral reaction cross section values with the experimental results for H^-, D_2 collisions at (a) $T_{rot} \sim 180$ K and (b) $T_{rot} = 300$ K.

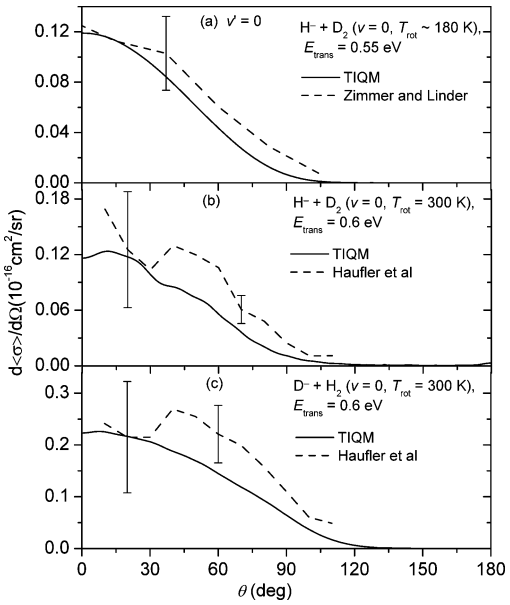

Figure 3. Plots of the computed *j*-weighted differential cross section values compared with the experimental results for (a) H^-, D_2 collisions for $v' = 0$, (b) H^-, D_2 collisions, and (c) D^-, H_2 collisions at the energies indicated.

$T_{rot.} \sim 180$ K. Our computed results of $\langle\sigma\rangle$ (E_{trans}) for H^-, D_2 collisions are shown to be in excellent agreement with the experimental results of Zimmer and Linder,[5] for energies up to 1.5 eV, in Figure 2a. Our calculated results of $\langle\sigma\rangle(E_{trans})$ at $T_{rot} = 300$ K for H^-, D_2 collisions are compared with the experimental results by Haufler et al.[7] in Figure 2b. The computed *j*-weighted integral reaction cross section values are comparable to the experimental results in the range $E_{trans} = 0.8-1.2$ eV. However, there are two discrepancies: (i) Experimental results suggest a lower threshold than the theoretical results. This seems to be typical of the results obtained from the guided ion beam technique.[7] A similar discrepancy was found for (He, H_2^+) also. (ii) Experimental results are lower than the theoretical results at higher energies, clearly due to the onset of an electron detachment channel, which is not included in our theoretical studies.

A.2. Differential Reaction Cross Sections. The differential reaction cross section values are also dependent on initial *j* (not shown). The *j*-weighted differential reaction cross section has been calculated from individual *j*-dependent differential cross section values as follows:

$$\frac{d\langle\sigma_{\alpha'v'j'k'\leftarrow avjk}\rangle}{d\Omega}(\theta) = \sum_j w_j(T_{rot.})\frac{d\sigma_{\alpha'v'j'k'\leftarrow avjk}}{d\Omega}(\theta) \qquad (20)$$

The product vibrational state (v') specific differential reaction cross section values have been calculated for $j = 0-4$ and $j = 0-3$ for H^-, D_2 ($v = 0$) and D^-, H_2 ($v = 0$) collisions, respectively. The *j*-weighted ($T_{rot} \sim 180$ K) differential reaction cross section values for (H^-, D_2) collisions at $E_{trans} = 0.55$ eV are compared with the experimental results of Zimmer and Linder[34] in Figure 3a. Clearly, the agreement between theory and experiment is excellent. The computed *j*-weighted differential cross section values at $T_{rot} = 300$ K and $E_{trans} = 0.6$ eV are compared with the experimental results of Haufler et al. in Figure 3b. It can be seen that the calculated differential cross section values are slightly lower than the experimental results. Similarly, the computed results for D^-, H_2 collisions at $T_{rot} = 300$ K and $E_{trans} = 0.6$ eV are shown to be comparable to the

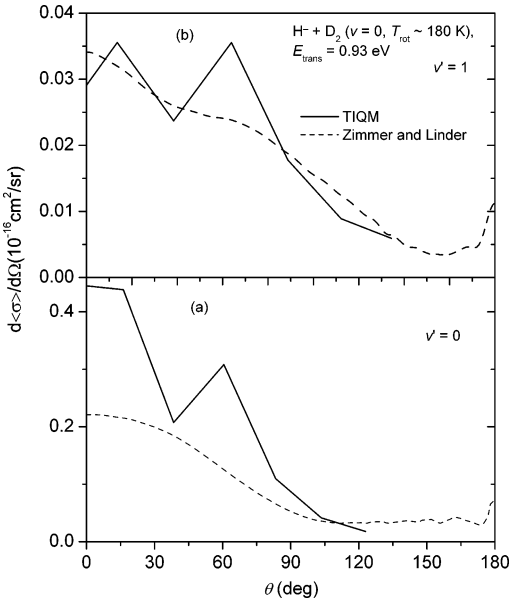

Figure 4. Comparison of the calculated *j*-weighted differential cross section values for H^-, D_2 collisions with the experimental results by Zimmer and Linder[34] for (a) $v' = 0$ and (b) $v' = 1$ at $E_{trans} = 0.93$ eV.

experimental results in Figure 3c. At $E_{trans} = 0.93$ eV, the computed *j*-weighted ($T_{rot} \sim 180$ K) differential reaction cross section values plotted for H^-, D_2 collisions for $v' = 0$ and 1 are comparable to the experimental results as illustrated in Figure 4. A more detailed comparison of the plots of the calculated *j*-weighted differential cross section values for H^-, D_2 for $v' = 0$, 1 and 2 at $E_{trans} = 1.16$ eV and $v' = 0$, 1, 2 and 3 at $E_{trans} = 1.48$ eV with the experimental results in Figure 5 reveal that the overall agreement between theory and experiment is excellent, except for some differences near $\theta = 0$.

B. TDQM Results. *B.1. Reaction Probabilities.* Initial-state-selected reaction probability (P^J_{vj}) values summed over different rotational and vibrational levels of the product diatom for the reactants H_2 ($j = 0-3$) and D_2 ($j = 0-4$) in $v = 0$ state were computed over a range of E_{trans} for each integer value of

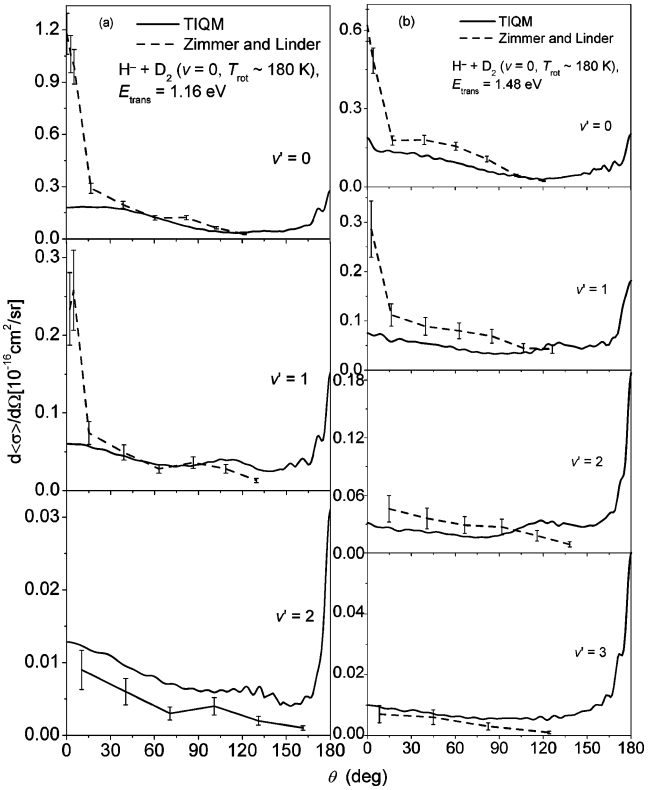

Figure 5. Comparison of the calculated *j*-weighted differential cross section values for H^-, D_2 collisions with the experimental results for (a) $v' = 0-2$ at $E_{trans} = 1.16$ eV and (b) $v' = 0-3$ at $E_{trans} = 1.48$ eV.

J in the range 0−50 for (H^-, D_2) collisions and 0−60 for (D^-, H_2) collisions. For both systems, for $J = 0$ and $j = 0$, the reaction probability obtained in the present study is nearly the same as the earlier reported probability values obtained using an L-shaped grid except for some oscillations. The reaction probability increases with an increase in E_{trans} dramatically near the threshold and then it increases further in steps, before leveling off or declining beyond 1.5 eV (not shown).

B.2. Reaction Cross Sections. From the results of P^J_{0j} (E) values computed for a range of J and $j = 0-4$ for H^-, D_2 collisions, the integral reaction cross section values were calculated using eq 17 and the resulting σ_{0j} values were plotted as a function of E_{trans} in Figure 6a. The value of σ_{0j} increases sharply at the threshold, reaches a maximum around 1.5 eV and then it declines slightly for all values of *j*. There is a sharp increase in σ in going from $j = 0$ to 1. But σ decreases with a further increase in *j* to 2, 3 and 4 to the extent that the σ values for $j = 3$ and 4 are lower than that for $j = 0$ for $E \leq 1.5$ eV. This strong dependence of σ on *j* indicates the strong influence of the anisotropy of the PES on the dynamics.[16] To understand the origin of the differences in the dependence of σ_{0j} on *j* for (H^-, D_2) collisions as obtained from TIQM (Figure 1) and TDQM ((CS), Figure 6a) calculations, σ_{0j} values are plotted as a function of E_{trans} for different *j* values in Figure 7. For $j = 0$, the TDQM results are in excellent agreement with the TIQM results. However, with an increase in *j*, the differences between the two sets of results become noticeable, with the largest difference arising for $j = 1$. A comparison of the TIQM results obtained for $k_{max} = 1$, 2 and 3 for $j = 1$ confirms that the TDQM results obtained with $k_{max} = 2$ can be considered as converged. This means that the differences between the TDQM (CS) and TIQM results arise from the neglect of Coriolis coupling in the TDQM calculations. Similar discrepancies have been noted for other systems like (He, H_2^+), particularly for $j = 1$.[35] Interestingly, the differences between TDQM (CS) and TIQM results become less marked for $j = 2$, 3 and 4, particularly for $E_{trans} \leq 1.0$ eV.

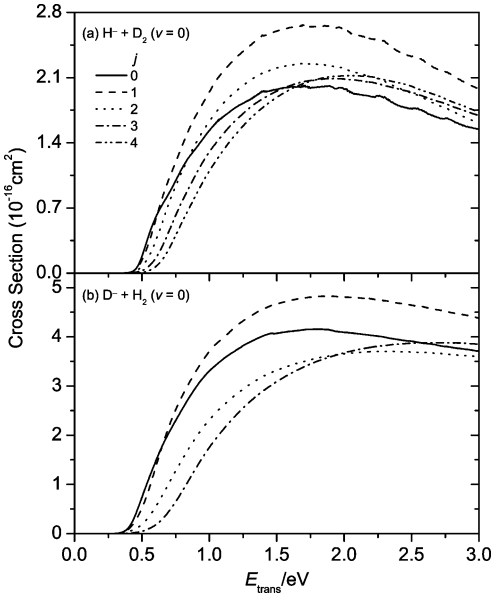

Figure 6. Computed TDQM reaction cross section values plotted as a function of E_{trans}/eV for different initial *j* values for (a) H^-, D_2 ($v = 0$) and (b) D^-, H_2 ($v = 0$) collisions.

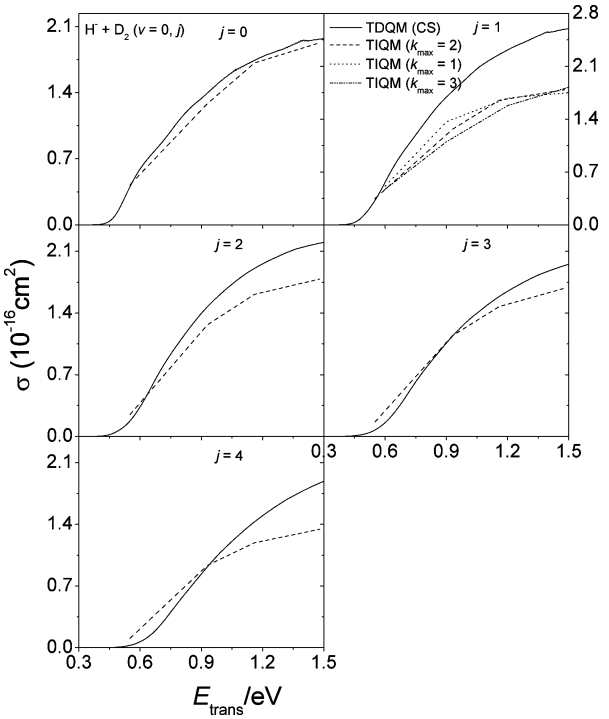

Figure 7. Comparison of the computed TDQM (CS) and TIQM results of σ ($v = 0$, *j*) for different values of *j* for H^-, D_2 ($v = 0$) collisions.

The *j*-weighted results obtained from TDQM (CS) calculations for H^-, D_2 collisions are compared with the experimental results of Zimmer and Linder[5] at $T_{rot} \sim 180$ K in Figure 8a. Although the TDQM results show the same qualitative trend as the experimental results, there are noticeable discrepancies between the two, at intermediate energies. Our calculated results of $\langle\sigma\rangle(E_{trans})$ at $T_{rot} = 300$ K for H^-, D_2 collisions are compared with the experimental results by Haufler et al.[7] in Figure 8b. As was noticed with the TIQM results, the experimental results show a lower threshold than the TDQM results. If the

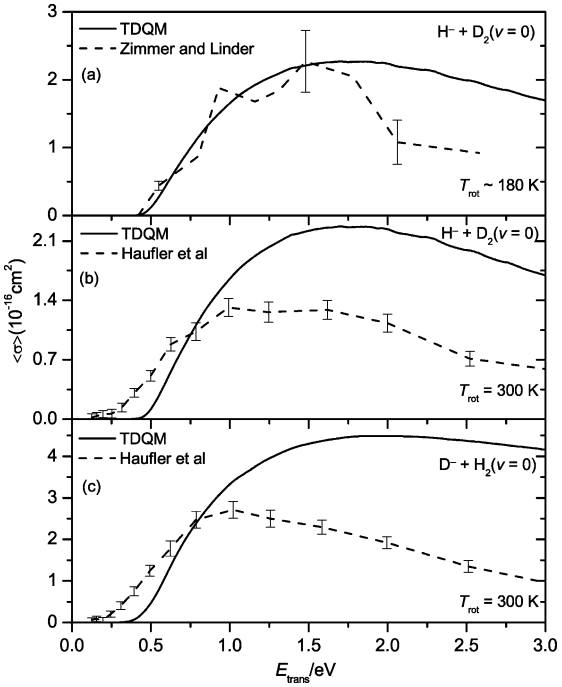

Figure 8. Comparison of the TDQM computed *j*-weighted integral reaction cross section values with the experimental results for (a) H^-, D_2 at $T_{rot} \sim 180$ K, (b) H^-, D_2 at $T_{rot} = 300$ K and (c) D^-, H_2 at $T_{rot} = 300$ K.

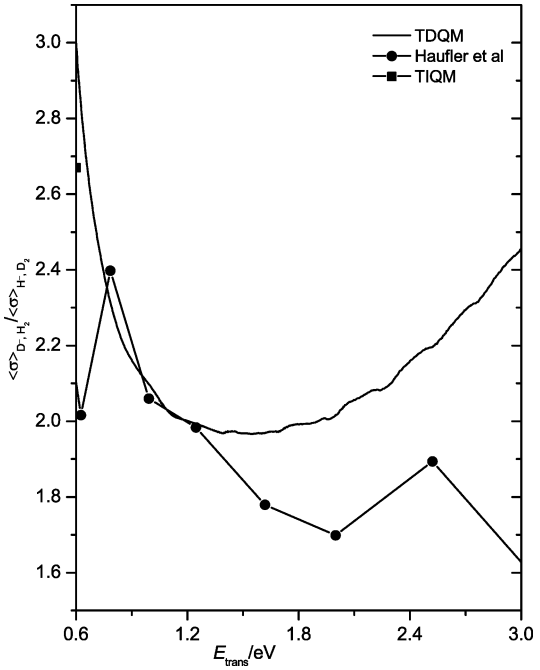

Figure 9. Comparison of the calculated ratio of the *j*-weighted reaction cross section values at $T_{rot} = 300$ K for D^-, H_2 to that of H^-, D_2 collisions with the experimental results by Haufler et al.[7]

experimental results were corrected by a 0.25 eV upward shift in the threshold energy, the agreement between theory and experiment would be excellent. As was mentioned earlier, the experimental $\langle\sigma\rangle$ values decline markedly with increase in E_{trans} beyond 1.5 eV because of the onset of electron detachment channel, which is not included in our theoretical studies.

The TDQM computed values of σ_{0j} for D^-, H_2 ($v = 0$, j) collisions are plotted as a function of E_{trans} in Figure 6b for $j = 0-3$. The influence of j and E_{trans} on σ_{0j} for D^-, H_2 ($v = 0$, j) collisions is similar to that for H^-, D_2 ($v = 0$, j). Yet it must be emphasized that the σ_{0j} values for the former system are a factor of 2 larger than those for the latter. The plot of $\langle\sigma\rangle$ for D^-, H_2 collisions in Figure 8c shows qualitatively the same behavior as $\langle\sigma\rangle$ for (H^-, D_2) in that the theoretical results start at a higher threshold than the experimental results and that the decline in $\langle\sigma\rangle$ with increase in E_{trans} is only marginal when compared to the steep decline in the experimental results.

As was mentioned earlier, the σ_{0j} values for (D^-, H_2) collisions are approximately a factor of 2 larger than those for (H^-, D_2). The *j*-weighted σ values computed for (D^-, H_2) are a factor of 2−3 larger than that for (H^-, D_2), as illustrated in Figure 9. The experimental results for $\langle\sigma\rangle(D^-, H_2)/\langle\sigma\rangle(H^-, D_2)$ are close to the computed values for $E_{trans} < 1.2$ eV, beyond which the two diverge from each other.

IV. Summary and Conclusion

The computed integral reaction cross section values for $H^- + D_2$ ($v = 0$, $j = 0-4$) and $D^- + H_2$ ($v = 0$, $j = 0-3$) show a noticeable dependence on the initial value of j for all the energies considered. The computed *j*-weighted integral reaction cross section values are shown to be in good agreement with the experimental results of Zimmer and Linder for $E \leq 2.0$ eV and lower than the results reported by Haufler et al. for $E \leq 1.5$ eV. The computed *j*-weighted differential reaction cross section results are also in good agreement with the experimental results at different relative translational energies for (H^-, D_2) collisions and at $E_{trans} = 0.6$ eV for (D^-, H_2) collisions.

Acknowledgment. We thank Dr. D. Skouteris for providing the integral and differential cross sections calculating codes. We are thankful to Dr. D. Gerlich for providing integral and differential reaction cross section values for comparison. K.G. is grateful to the Council of Scientific and Industrial Research (CSIR), New Delhi, for a Fellowship. This study was supported in part by a grant from CSIR, New Delhi. N.S. thanks the Department of Science and Technology, New Delhi, for the J. C. Bose fellowship.

References and Notes

(1) Muschlitz, E. E., Jr.; Bailey, T. L.; Simons, J. H. *J. Chem. Phys.* **1956**, *24*, 1202; **1957**, *26*, 711.
(2) Mason, E. A.; Vanderslice, J. T. *J. Chem. Phys.* **1958**, *28*, 1070.
(3) Michels, H. H.; Paulson, J. F. In *Potential Energy Surface and Dynamics Calculations*; Truhlar, D. G., Ed.; Plenum: New York, 1981.
(4) Huq, M. S.; Doverspike, L. D.; Champion, R. L. *Phys. Rev. A* **1982**, *27*, 2831.
(5) Zimmer, M.; Linder, F. *Chem. Phys. Lett.* **1992**, *195*, 153. Zimmer, M.; Linder, F. *J. Phys. B* **1995**, *28*, 2671.
(6) Müller, H.; Zimmer, M.; Linder, F. *J. Phys. B* **1996**, *29*, 4165.
(7) Haufler, E.; Schlemmer, S.; Gerlich, D. *J. Phys. Chem. A* **1997**, *101*, 6441.
(8) Belyaev, A. K.; Colbert, D. T.; Groenenboom, G. C.; Miller, W. H. *Chem. Phys. Lett.* **1993**, *209*, 309.
(9) Stärck, J.; Meyer, W. *Chem. Phys.* **1993**, *176*, 83.
(10) Belyaev, A. K.; Tiukanov, A. S. *Chem. Phys. Lett.* **1999**, *302*, 65.
(11) Mahapatra, S.; Sathyamurthy, N.; Kumar, S.; Gianturco, F. A. *Chem. Phys. Lett.* **1995**, *241*, 223.
(12) Gianturco, F. A.; Kumar, S. *J. Chem. Phys.* **1995**, *103*, 2940.
(13) Mahapatra, S.; Sathyamurthy, N. *J. Phys. Chem.* **1996**, *100*, 2759. Mahapatra, S.; Sathyamurthy, N. *Faraday Discuss. Chem. Soc.* **1998**, *110*, 228.
(14) Ansari, W. H.; Sathyamurthy, N. *Chem. Phys. Lett.* **1998**, *289*, 487.
(15) Mahapatra, S. *Phys. Chem. Chem. Phys.* **2000**, *2*, 671.
(16) Jaquet, R.; Heinen, M. *J. Phys. Chem. A* **2001**, *105*, 2738.
(17) Morari, C.; Jaquet, R. *J. Phys. Chem. A* **2005**, *109*, 3396−9343.
(18) Panda, A. N.; Sathyamurthy, N. *J. Chem. Phys.* **2004**, *121*, 9343.
(19) Panda, A. N.; Giri, K.; Sathyamurthy, N. *J. Phys. Chem. A* **2005**, *109*, 2057.

(20) Giri, K.; Sathyamurthy, N. *J. Phys. B: At. Mol. Opt. Phys.* **2006**, *39*, 4123.
(21) Aguado, A.; Tablero, C.; Paniagua, M. *Comput. Phys. Commun.* **1998**, *108*, 259.
(22) Skouteris, D.; Castillo, J. F.; Manolopoulos, D. E. *Comput. Phys. Commun.* **2000**, *133*, 128.
(23) Balakrishnan, N.; Kalyanaraman, C.; Sathyamurthy, N. *Phys. Rep.* **1997**, *280*, 79.
(24) Zhang, J. Z. H. *Theory and Application of Quantum Molecular Dynamics*; World Scientific: Singapore, 1999.
(25) Mohan, V.; Sathyamurthy, N. *Comput. Phys. Rep.* **1988**, *7*, 213.
(26) Marston, C. C.; Balint-Kurti, G. G. *J. Chem. Phys.* **1989**, *91*, 3571.
(27) Kosloff, D.; Kosloff, R. *J. Chem. Phys.* **1983**, *52*, 35.
(28) Lill, J. V.; Light, J. C. *Chem. Phys. Lett.* **1982**, *89*, 483. Light, J. C.; Hamilton, I.P.; Lill, J. V. *J. Chem. Phys.* **1985**, *82*, 1400.
(29) Pack, R T. *J. Chem. Phys.* **1974**, *60*, 633.
(30) Feit, M. D.; Fleck, J. A., Jr.; Steiger, A. *J. Chem. Phys.* **1982**, *47*, 412.
(31) Kalyanaraman, C.; Clary, D. C.; Sathyamurthy, N. *J. Chem. Phys.* **2000**, *113*, 59.
(32) Mahapatra, S.; Sathyamurthy, N. *J. Chem. Soc., Faraday Trans.* **1997**, *93*, 773.
(33) Sathyamurthy, N. *Chem. Rev.* **1983**, *83*, 601.
(34) As obtained from Gerlich, D. Private Communication.
(35) Chu, T.-S.; Lu, R.-F.; Han, K.-L.; Tang, X.-N.; Xu, H.-F.; Ng, C. Y. *J. Chem. Phys.* **2005**, *122*, 244322.